RSC Advances

PAPER

View Article Online
View Journal | View Issue

Cite this: *RSC Adv.*, 2026, **16**, 8371

6,6′-Biazulenic core as a platform for unlocking Hammett constants *via* electrochemical free-energy relationships

Joseph A. Mandigo, †[a] Shaun R. Kelsey, †[a] Jason C. Applegate, [a] Rene C. Sabala, [a] Monisola K. Dairo, [a] Carben R. Weghorn, [a] Raina Fair,[a] Cindy L. Berrie, *[a] Ward H. Thompson, *[a] Daron E. Janzen [b] and Mikhail V. Barybin *[a]

Quantitative appreciation of electronic substituent effects is beneficial across the chemical sciences, from reaction kinetics and catalysis to functional materials design and enzymatic processes. While Hammett parameters (σ constants) constitute the most widely invoked paradigm, their determination for structurally complex functional groups is often impractical by traditional empirical means. Herein, we demonstrate that the reversible one-step, 2-e$^-$ reduction of linearly functionalized 1,1′,3,3′-tetraethoxycarbonyl-6,6′-biazulene provides a simple electrochemical readout of effective Hammett constants. By design, the values obtained align closely with the conventional σ_p descriptors pertaining to benzenoid systems. This approach not only helps reevaluate previously reported Hammett values but also quantifies the role of intramolecular hydrogen bonding (*e.g.*, C═O···H–S) and enables determining effective σ constants (σ_{eff}) for "designer" functional groups, such as –SAuPPh$_3$ and –NCCr(CO)$_5$. Moreover, the long-range net electron donor/acceptor influence of the substituents –S$^-$, –SAuPPh$_3$, –SH, –SCH$_2$CH$_2$CO$_2$CH$_2$CH$_3$, and –NCCr(CO)$_5$ on the [(–NC)Cr(CO)$_5$] ^{13}C NMR reporter across the 6,6′-biazulenic π-linker was unveiled through inverse-linear $\delta(^{13}CO_{trans})$ *vs.* $\delta(^{13}CN)$ and $\delta(^{13}CO_{cis})$ *vs.* $\delta(^{13}CN)$ correlations. The π-communication along the molecular axis of the 6,6′-biazulenic scaffold was further confirmed *via* Reflection-Absorption Infrared (RAIR) spectroscopic analysis of [(OC)$_5$Cr(η^1-2-isocyano-2′-mercapto-1,1′,3,3′-tetraethoxycarbonyl-6,6′-biazulene)] self-assembled on the Au(111) surface. By uniting redox tunability with rigorous linear free-energy correlations, this work offers both a versatile molecular platform and a straightforward electrochemical strategy for expanding and refining the Hammett parameter domain.

Received 6th January 2026
Accepted 4th February 2026

DOI: 10.1039/d6ra00120c

rsc.li/rsc-advances

Introduction

Hammett parameters have long provided a quantitative language for describing how functional groups modulate the electronic landscape of molecular scaffolds across diverse areas of chemistry, from reaction kinetics[1–3] and catalysis[4–6] to enzymatic processes[7–9] and design of functional materials[6,10–12] and pharmaceuticals.[13,14] Also referred to as σ constants, these parameters were originally conceived to quantify the influence of *para*- or *meta*-ring substituents on the ionization equilibria of benzoic acids and remain the most widely applied metric of substituent electronic effects in aromatic compounds.[1–14] The recent resurgence of experimental[1,6,15–17] and computational efforts[18–25] aimed at broadening and reevaluating this intuitively appealing chemical parameter space underscores the need for robust methodologies capable of addressing "designer" substituents, for which σ descriptors are currently unavailable. There are also some persistent ambiguities in the Hammett constant values for certain substituents.[1,26] For example, there is little consensus on the σ_p constant for the –NMe$_2$ group, with various authors suggesting values in the range of −0.21 to −1.05.[27] The most frequently cited value of −0.83 was derived by McDaniel[28] in 1957 from the classical ionization data for *para*-dimethylaminobenzoic acid reported by Johnston[29] in 1906 (31 years before introduction of the Hammett equation).

To address the above challenges, our group has turned to 6,6′-biazulene—a π-extended, nonbenzenoid aromatic framework featuring two linearly connected azulenyl units—as a molecular platform for quantifying substituent effects. 6,6′-Biazulene (Fig. 1a) exhibits complementary orbital density distributions in its frontier molecular orbitals: the Highest Occupied Molecular Orbital (HOMO) is distributed over the

[a]*Department of Chemistry, University of Kansas, Lawrence, KS 66045, USA. E-mail: mbarybin@ku.edu; cberrie@ku.edu; wthompson@ku.edu*

[b]*Department of Chemistry and Biochemistry, St. Catherine University, St. Paul, MN 55105, USA*

† J. A. M. and S. R. K. contributed equally to this work.

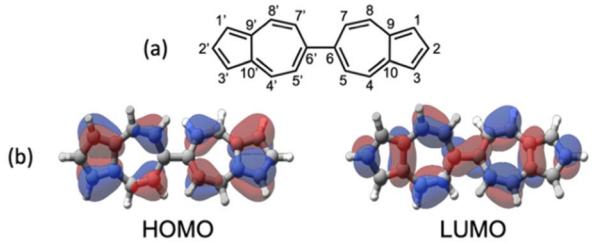

Fig. 1 (a) 6,6′-Biazulene and its atom numbering scheme. (b) Highest occupied and lowest unoccupied molecular orbitals of 6,6′-biazulene.

odd-numbered carbon atoms, whereas the Lowest Unoccupied Molecular Orbital (LUMO) has a π* topology with non-zero orbital density at the even-numbered positions (Fig. 1b). Consequently, functionalization at the 2,2′-carbon atoms of the 6,6′-biazulenic scaffold selectively perturbs the energy of the LUMO whilst leaving the HOMO largely unaffected, therefore enabling tunability of the platform's reduction potential.

Of special note, the one-step, two-electron reduction of the 6,6′-biazulenic core[30–35] proceeds under a rare regime of reduction potential inversion.[36–38] Such distinctive behaviour not only simplifies the electrochemical readout by yielding a single, well-defined redox couple but also enhances the sensitivity of the system to even subtle substituent-induced perturbations in electronic structure. To the best of our knowledge, the 6,6′-biazulenic scaffold is the only one among currently accessible positional biazulene isomers[39] that supports a one-step, two-electron reduction profile. Fig. 2 shows that the sum of literature σ_p values for our original series[40] of seven symmetrically and unsymmetrically substituted derivatives of 1,1′,3,3′-tetraethoxycarbonyl-6,6′-biazulene varies linearly with the half-wave potentials ($E_{1/2}$), providing a reliable calibration plot that anchors the study reported herein. The intrinsic boundaries of the relationship are determined by the $CH_2Cl_2/^nBu_4NPF_6$ electrolyte solution window used in our electrochemical studies (*ca.* −2 to +2 V *vs.* SCE with $E_{1/2}(Cp_2Fe^0/Cp_2Fe^+) = 0.46$ V).[41,42]

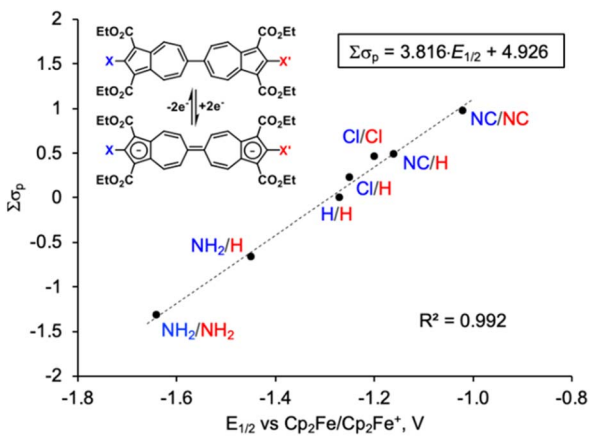

Fig. 2 A plot of the combined σ_p Hammett parameters of the substituents *X* and *X′ vs.* the half-wave potential ($E_{1/2}$) for the 2-e$^-$ reduction of 2,2′-functionalized 6,6′-biazulenes.

Notably, the σ_p values used in this plot were determined from the experiments conducted in aqueous media, such that the σ_p constant of −0.66 (ref. 26) for the –NH_2 substituent inherently includes the contribution from solvation-induced hydrogen bonding. On the other hand, 2,2′-diamino-1,1′,3,3′-tetraethoxy-carbonyl-6,6′-biazulene engages in intramolecular H-bonding interactions between its amino and carboxylic ester groups, as evidenced by a markedly deshielded ^{1}H NMR resonance at $\delta(NH_2) = 7.88$ ppm[34] compared to 4.58 ppm for 2-aminoazulene in $CDCl_3$ (Fig. S29). Thus, the H-bonding in this molecule may be regarded as a structural surrogate for solvent-mediated stabilization affecting the –NH_2 functional group in aqueous environments.

Building on this recently established linear free-energy relationship, we set out to implement the reverse Hammett analysis by considering electrochemical signatures of the 1,1′,3,3′-tetraethoxycarbonyl-6,6′-biazulenic core to extract effective σ values (σ_{eff}) for electronically and structurally complex functional groups such as –$SAuPPh_3$ and –$NCCr(CO)_5$ that should map directly onto the conventional σ_p scale.

Results and discussion

Synthesis and characterization of symmetrically and asymmetrically 2,2′-functionalized 6,6′-biazulenes

Recognizing the untapped synthetic potential of 2,2′-dichloro-1,1′,3,3′-tetraethoxycarbonyl-6,6′-biazulene (**1**)[40] for 2,2′-functionalization, we targeted the corresponding bis-mercapto-terminated derivative, a structural motif well-suited for interfacing π-conjugated linkers with metal atoms and surfaces. Refluxing **1** with ethyl 3-mercaptopropionate in pyridine displaced both chlorine substituents, furnishing the isolable, albeit somewhat oily, dark purple-brown intermediate **2** (Scheme 1). Subsequent base hydrolysis of **2**, followed by acidification, afforded 2,2′-dimercapto-1,1′,3,3′-tetraethoxy-

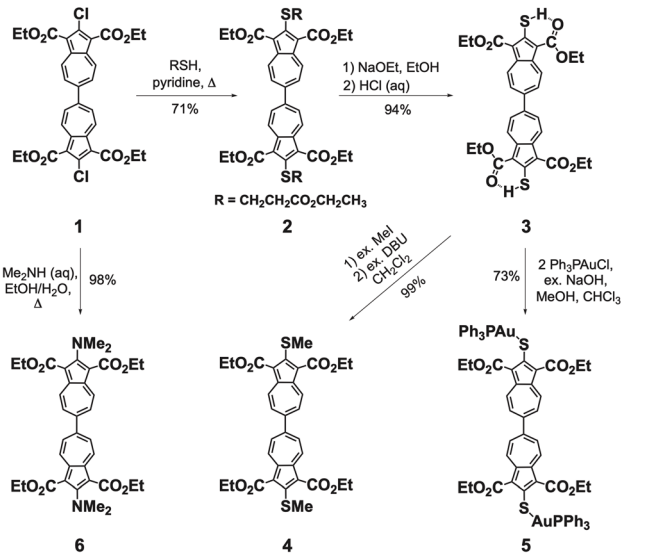

Scheme 1 Syntheses of 6,6′-biazulenes symmetrically functionalized along their molecular axis.

carbonyl-6,6′-biazulene (**3**) as a brick-red microcrystalline solid. Similar to 2-mercapto-1,3-diethoxycarbonylazulene,[43] compound **3** engages in intramolecular C=O···H–S hydrogen bonding in both solution and solid state, as evidenced by a substantially deshielded mercapto ^{1}H NMR resonance (δ = 7.78 ppm in $CDCl_3$, Table S2), a low energy ν_{SH} stretch at 2474 cm^{-1}, and two distinct $\nu_{C=O}$ bands at 1689 and 1653 cm^{-1} (KBr pellet). Deprotonation of **3** with excess 1,8-diazabicyclo [5.4.0]undec-7-ene (DBU) generated the deeply purple-coloured dianionic intermediate **3***, which underwent clean methylation to give microcrystalline, dark red 2,2′-methylthio-1,1′,3,3′-tetraethoxy-carbonyl-6,6′-biazulene (**4**) in quantitative yield.

The ^{1}H NMR resonances for $H^{4,4',8,8'}$ and $H^{5,5',7,7'}$ in **3*** appear substantially upfield relative to those of either **3** or **4** (Fig. 3). Although the direct synthesis of **4** *via* nucleophilic substitution of the Cl termini in **1** using NaSMe (1 : 2) is conceptually feasible,[44] the operational drawbacks associated with the notoriously malodorous NaSMe reagent render the three-step, high-yielding sequence **1** → **2** → **3** → **4** the more practical alternative. In contrast to the methylation, treatment of *in situ*-generated **3*** with 2 equiv. of Ph_3PAuCl produced a bright red solution of the bimetallic complex **5**, which crystallized as a lustrous dark yellow solid (Scheme 1).

The solid-state structure of **4** reveals a three-component disorder of one of its SMe substituents with 50 : 31 : 19 positional occupancies (Fig. S57). The major conformer is depicted in Fig. 4. The interplanar angle between the two azulenic units of 39.7(3)° in **4** is the most acute among such parameters documented for all other crystallographically characterized 6,6′-biazulenes (typical range: 43.5–66.9°).[40] This comparison, however, should be interpreted with caution, as such torsional parameters are inherently influenced by crystal-packing forces. The SMe groups themselves are mildly twisted relative to the adjoining 2-azulenyl units, with dihedral angles of *ca.* 26 ± 1° in the major conformer.

Inspired by Nozoe's classical preparation of 2-(*N*,*N*-dimethylamino)-1,3-diethoxycarbonylazulene,[45] refluxing a purple solution of **1** with dimethylamine in EtOH/H_2O cleanly delivered 2,2′-(*N*,*N*-dimethylamino)-1,1′,3,3′-tetraethoxy-carbonyl-6,6′-biazulene (**6**) upon workup. Unlike many other 6,6′-biazulenes, this blood-red, air- and thermally-stable solid displays surprisingly good solubility in most organic solvents.

Schemes 2 and 3 outline our modular access to asymmetrically 2,2′-functionalized 6,6′-biazulenes that capitalizes on the Suzuki–Miyaura cross-coupling approach.[46] Purple-coloured 2-chloro-1,3-diethoxycarbonyl-6-pinacolato-borylazulene (**7**)[47] served as a convenient precursor to access scarlet 2-ethoxycarbonylethylthio-1,3-diethoxycarbonyl-6-iodoazulene (**9**) *via* isolable dark purple 2-ethoxycarbonyl-ethylthio-1,3-diethoxycarbonyl-6-pinacolatoborylazulene intermediate (**8**). Coupling of **7** and **9** under $Pd(PPh_3)_4$ catalysis provided dark red **10**, bearing $SCH_2CH_2CO_2Et$ and Cl substituents along the molecular axis. Further, sand-brown 2-mercapto-2′-chloro-6,6′-biazulene **11** and dark maroon 2-methylthio-2′-chloro-6,6′-biazulene **12** were prepared from **10** using the methods established above for the syntheses of **3** and **4**, respectively (Scheme 2).

Syntheses of 6,6′-biazulenes featuring the [(–NC)Cr(CO)$_5$] spectroscopic reporter at one of their termini are shown in Scheme 3. The Pd^0-catalyzed cross coupling of bright orange (OC)$_5$Cr(2-isocyano-1,3-diethoxycarbonyl-6-bromoazulene)[48] with **8** afforded the corresponding deep brown biazulenic

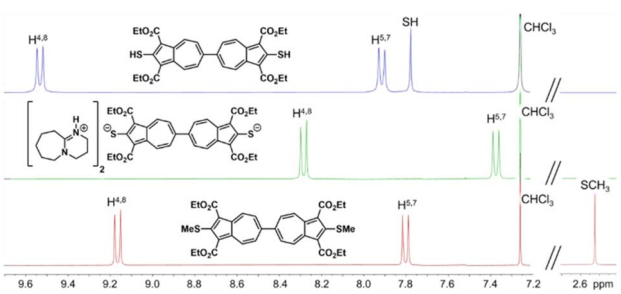

Fig. 3 ^{1}H NMR spectra of **3**, **3***, and **4** in $CDCl_3$ at 25 °C.

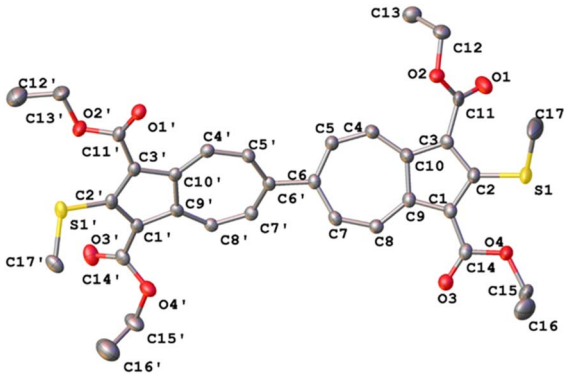

Fig. 4 Molecular structure of **4** (50% thermal ellipsoids). This is the major contributor to the three-component disordered structure illustrated in Fig. S57. Selected bond distances (Å) and angles (°): S1′–C2′ 1.745(3), S1–C2 1.756(7), C6′–C6 1.502(3), C5–C6–C6′–C5′ 39.7(3), C17′–S1′–C2′–C1′ 26.9(3).

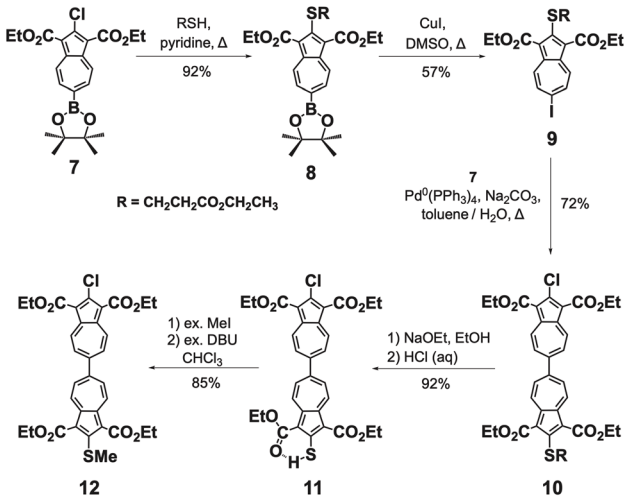

Scheme 2 Syntheses of 6,6′-biazulenes asymmetrically functionalized along their molecular axis.

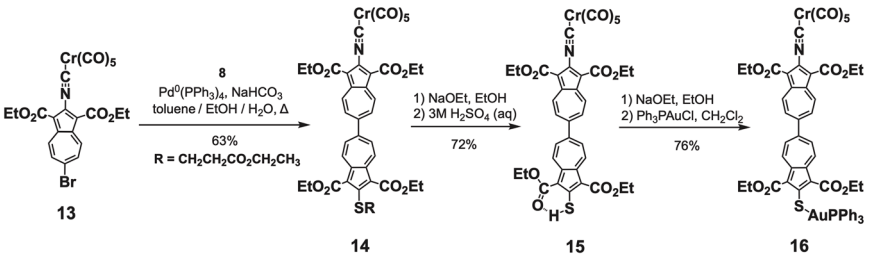

Scheme 3 Synthesis and metalation of the 2-isocyano-2′-mercapto-6,6′-biazulenic motif.

intermediate **14**, which was then converted to brown 2-isocyano-2′-mercapto-6,6′-biazulene derivative **15**. Species **15** represents an exceedingly scarce example of a compound containing both mercapto- and isocyano functionalities in the same molecule.[48] Metalation of the SH terminus of **15** with Ph_3PAuCl in the presence of NaOEt gave the plum-coloured heterobimetallic Cr^0/Au^I complex **16**.

Electrochemical mapping of substituent effects

We begin by examining the electrochemical consequences of mercapto substitution. The –SH functional group is especially attractive because it provides access to thiolate junctions relevant to molecular scale charge transport.[49] The half-wave potential of −1.31 V associated with the two-electron reduction of dimercaptobiazulene **3** translates, *via* the calibration plot in Fig. 2, to an effective Hammett constant $\sigma_{eff} = -0.04$ for the –SH substituent (Tables 1 and S4). This value represents a significant negative shift relative to the classical $\sigma_p(SH) = +0.15$ reported in the literature,[26,28] implying that the mercapto groups in **3** display subtle net electron-donating behavior rather than the weak electron-withdrawing character traditionally ascribed to S–H substituents. We attribute this discrepancy to intramolecular S–H···O=C hydrogen-bonding interactions[43,50] present in **3**. Consistent with this hypothesis, our DFT calculations indicate that disrupting such H-bonding interactions (modeled by rotating each S–H bond out of the plane of the corresponding azulenyl unit) lowers the energy of the biazulene LUMO (Fig. S59). To probe the role of the above hydrogen bonding experimentally, we replaced the hydrogen atoms of the –SH groups with methyl substituents. The resulting bis(methylthio)-substituted biazulene **4** undergoes a two-electron reduction at $E_{1/2} = -1.30$ V, corresponding to $\sigma_{eff}(SMe) = -0.03$. This value closely matches $\sigma_p(SMe) = 0.0$ originally reported by McDaniel[28] and later compiled in the comprehensive Hammett parameter tables by Hansch,[26] lending further support to our interpretation.

Importantly, the $E_{1/2}$ potential associated with the 2-e$^-$ reduction of asymmetrically –SH/–Cl functionalized biazulene **11** constitutes the average of the $E_{1/2}$ values determined for the

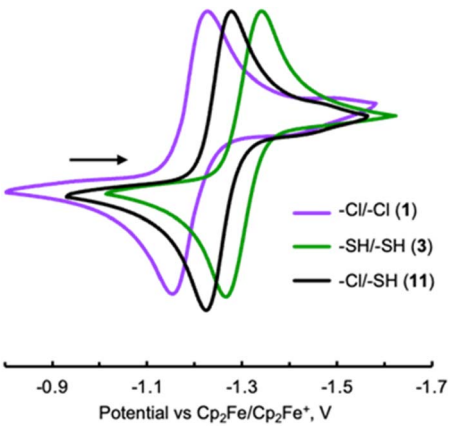

Fig. 5 Cyclic voltammograms of **1** (purple), **3** (green), and **11** (black) in 0.1 M $[^nBu_4N]^+[PF_6]^-/CH_2Cl_2$ *vs.* external $Cp_2Fe^{0/+}$ at 22 °C. Scan rate 100 mV s^{-1}.

Table 1 Predicted Hammett parameters for $-NMe_2$, –SH, $-SAuPPh_3$, and $-NCCr(CO)_5$ substituents based on the experimental $E_{1/2}$ values for the 2-e$^-$ reduction of 6,6′-biazulenes **3**, **4**, **5**, **6**, and **17**[a]

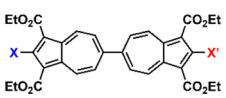

	X = X′	$E_{1/2}$, V (measured)	σ_{eff} (X) (predicted)
3	–SH	−1.31	−0.04
4	–SMe	−1.30	−0.03
5	$-SAuPPh_3$	−1.48	−0.36
6	$-NMe_2$	−1.59	−0.57
17	$-NC-Cr(CO)_5$	−1.00[a]	+0.56

[a] Ref. 35.

symmetrically substituted 2,2′-dimercapto and 2,2′-dichloro derivatives **1** and **3** (Fig. 5, Tables 1, 2, and S4). Similarly, the reduction of **12** featuring asymmetric –SMe/–Cl substitution is exactly half-way between those of **1** and **4** (Tables 1 and 2).

Linear free-energy relationships are rarely stress-tested against substituents that fall well outside the classical functional group palette. To assess the limits and transferability of the correlation uncovered in Fig. 2, we therefore extended our electrochemical Hammett analysis to 6,6′-biazulenes bearing "designer" substituents –$SAuPPh_3$ and –$NCCr(CO)_5$. These moieties are anticipated to exert very different net electron donating/withdrawing influences. Notably, our previous X-ray crystallographic analyses of several complexes featuring the $(OC)_5Cr$(2-isocyano-1,3-diethoxycarbonylazulene) motif indicate that the C–N–C–Cr unit invariably assumes a nearly linear geometry, with minimal steric hindrance between the CO_2Et and $Cr(CO)_5$ fragments.[35,48,51–53] The 6,6′-biazulene **5** featuring –$SAuPPh_3$ termini undergoes reduction at $E_{1/2} = -1.48$ V, which allowed to extract the σ_{eff} value of −0.36 for the –$SAuPPh_3$ substituent. This quantitative observation reflects the significantly enhanced net electron-donating character of –$SAuPPh_3$ *vs.* –SH (Tables 1 and S4). On the other hand, reduction of the 6,6′-biazulenic core terminated with –$NCCr(CO)_5$ groups along its molecular axis in **17** occurs at $E_{1/2} = -1.00$ V,[35] which yields $\sigma_{eff}[-NCCr(CO)_5] = +0.56$. This is consistent with the $Cr(CO)_5$ fragment exerting a net electron withdrawing effect on the isocyano substituent (*cf.* $\sigma_p = +0.49$ (ref. 26) for the uncomplexed isocyano group). The 9 cm^{-1} hypsochromic shift of the ν_{NC} IR band upon complexation of free 2,2′-diisocyano-1,1′,3,3′-tetraethoxy-carbonyl-6,6′-biazulene ($\nu_{NC} = 2127$ cm^{-1} in CH_2Cl_2) to form homobimetallic **17** ($\nu_{NC} = 2136$ cm^{-1} in CH_2Cl_2) nicely mirrors the above conclusion as well.[34,35]

To test whether the σ_{eff} constants for –$SAuPPh_3$ and –$NCCr(CO)_5$ would abide the linear free-energy paradigm established by the calibration plot in Fig. 2, we considered the 2-e^- reduction behaviour of asymmetrically-functionalized 6,6′-biazulenes **15**, **16**, and **18** (Tables 2 and S4). The one-step, 2-e^- reduction of **15** bearing the –$NCCr(CO)_5$ and –SH groups along its molecular axis occurs at −1.16 V. Gratifyingly, this value is precisely the average of the $E_{1/2}$ potentials that we documented for the reductions of symmetrically-substituted congeners **3** and **17**. Similarly, **18** undergoes reduction at $E_{1/2} = -1.14$ V, which is exactly in between the $E_{1/2}$ values observed for the reductions of **17** and 1,1′,3,3′-tetraethoxycarbonyl-6,6′-biazulene.[40] Finally, the heterobimetallic species **16** is reduced at $E_{1/2} = -1.24$ V—quite close to the predicted value of −1.26 V inferred from the redox profiles of homobimetallic **5** and **17** (Tables 1 and 2).

We next turned to dimethylamino substitution, which represents a canonical class of strong π-electron donors in classical Hammett analyses.[26] Examination of the –NMe_2-functionalized biazulene allows a direct comparison between established substituent expectations and the experimentally observed redox response. This case is particularly intriguing because steric repulsion between the –NMe_2 and –CO_2Et groups in **6** twists the –NMe_2 substituents out of optimal π-conjugation with the biazulenic core by *ca.* 32 ± 2° (Fig. 6), thereby likely diminishing their mesomeric electron-donating contributions to σ_{eff}. The $E_{1/2}$ potential associated with the 2-e^- reduction of the bis(*N*,*N*-dimethylamino) derivative **6** is 50 mV less negative than that documented for 2,2′-diamino-1,1′,3,3′-tetraethoxycarbonyl-6,6′-biazulene[34] (Table 1 and Fig. 7). According to our calibration plot in Fig. 2, the effective Hammett σ constant for the –NMe_2 substituent is predicted to be −0.57, which is identical to the σ_p value of −0.574 obtained by Gilman and Dunn[54] through the alkaline hydrolysis of *p*-*N*,*N*-dimethylamino functionalized ethyl benzoate. However, the fact that **6** is easier to reduce than its diamino-functionalized

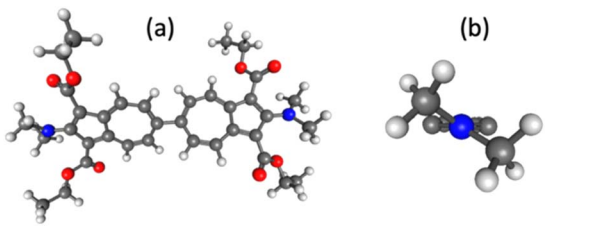

Fig. 6 (a) DFT-optimized molecular structure of **6** (B3LYP/6-31+G*, CH_2Cl_2 medium). (b) A Newman projection of a Me_2N-azulenyl moiety with the CO_2Et groups truncated.

Table 2 Measured *vs.* predicted $E_{1/2}$ values for the 2-e^- reduction of asymmetrically functionalized 6,6′-biazulenes **11**, **12**, **15**, **16**, and **18** [a,b]

	X X′	σ_{eff}(X) + σ_{eff}(X′)	$E_{1/2}$, V (predicted)	$E_{1/2}$, V (measured)
11	–Cl –SH	0.23[a] + (−0.04) = 0.19	−1.24	−1.25
12	–Cl -SMe	0.23[a] + (−0.03) = 0.20	−1.24	−1.24
15	-$NCCr(CO)_5$ –SH	0.56 + (−0.04) = 0.52	−1.16	−1.16
16	–$NCCr(CO)_5$ –$SAuPPh_3$	0.56 + (−0.36) = 0.20	−1.24	−1.26
18	–$NCCr(CO)_5$ –H	0.56 + 0.00[a] = 0.56	−1.14	−1.14[b]

[a] Ref. 26. [b] Ref. 35.

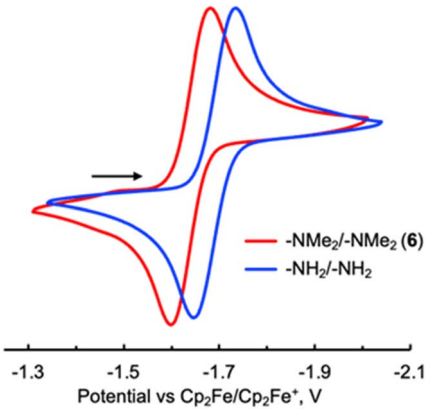

Fig. 7 Cyclic voltammograms of **6** (red) and 2,2′-diamino-1,1′,3,3′-tetraethoxycarbonyl-6,6′-biazulene (blue) in 0.1 M $[^{n}Bu_4N]^+[PF_6]^-$/CH_2Cl_2 *vs.* external $Cp_2Fe^{0/+}$ at 22 °C. Scan rate 100 mV s^{-1}.

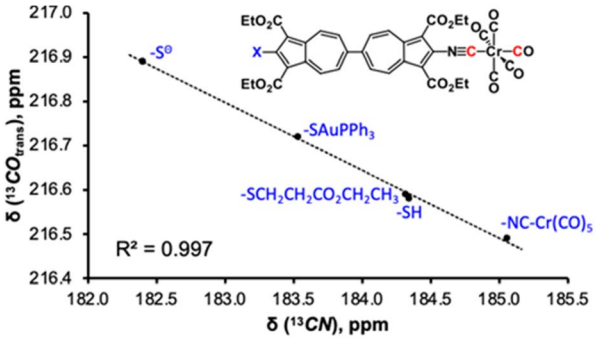

Fig. 8 Plot of $\delta(^{13}CO_{trans})$ *vs.* $\delta(^{13}CN)$ chemical shifts (in $CDCl_3$) for the [–NCCr(CO)$_5$] moiety in complexes of functionalized 2-isocyanobiazulene ligands.

congener may be perceived as counterintuitive in light of the typical view that $-NMe_2$ is a stronger net electron donor than $-NH_2$. This observation can be rationalized by two factors that affect $E_{1/2}$ in opposite directions. First, intramolecular hydrogen-bonding interactions in 2,2′-diamino-1,1′,3,3′-tetraethoxycarbonyl-6,6′-biazulene render the $-NH_2$ substituents more electron donating, which further raises the energy of this biazulene's LUMO. Second, the steric congestion illustrated in Fig. 6 somewhat weakens π-conjugation of the $-NMe_2$ groups with the biazulenic scaffold. Such mode of steric and conformational attenuation of donor strength echoes Nozoe's observation that 2-(*N*,*N*-dimethylamino)-1,3-diethoxycarbonylazulene is inert toward electrophilic aromatic substitution with Br_2 at the 6-position of the azulenic core, whereas 2-aminoazulene easily undergoes such bromination.[45,51] Moreover, in the electrochemical context, Stahl, Hammes–Schiffer, and co-workers showed that bulky substituents at the 2,3- or 5,6-positions of quinones led to one-electron reduction potentials that are shifted to more positive values than anticipated from linear Hammett correlations.[6]

Correlating ^{13}C NMR signatures of the [(–NC)Cr(CO)$_5$] reporter with remote substituent effects

In their earlier studies, Figueroa and co-workers explored the [Cr(CO)$_5$] fragment as a spectroscopic handle for evaluating the σ-donor/π-acceptor balance of isocyanide ligands through inverse-linear correlations between the ^{13}C chemical shifts of *trans*- or *cis*-carbonyl ligands and the corresponding *k*(*trans*-CO) or *k*(*cis*-CO) force constants in (OC)$_5$Cr(CNR) complexes.[55] Although this approach differentiated quite successfully between isocyanide ligands with strongly contrasting non-aryl-based substituents *R*, the authors acknowledged its limited utility in the context of functionalized aryl isocyanides, suggesting that the aryl moiety imposes a leveling effect on the substituent's intrinsic electronic character. Moreover, the precision of this analysis diminished when the variations in the nature of *R* were subtle, owing to inherent uncertainties in extracting *k*(CO) values from ν_{CO} vibrational data for C_{4v}-symmetric M(CO$_5$)L.[47,56] More recently, we capitalized on the pronounced polarizability of azulene's π-system[57] to develop a highly sensitive ^{13}C NMR method that underpins the net σ-donor/π-acceptor character of functionalized 2-isocyanoazulenes from inverse-linear $\delta(^{13}CO_{trans})$ or $\delta(^{13}CO_{cis})$ *versus* $\delta(^{13}CN)$ correlations for (OC)$_5$Cr(2-isocyanoazulene) species.[48,52] Building upon this foundation, we now demonstrate that the [(–NC)Cr(CO)$_5$] unit serves as an exceptionally responsive ^{13}C NMR reporter capable of discerning electron delocalization mediated by a linear 6,6′-biazulenic π-linker over *ca.* 2 nm range.

Table S3 and Fig. 8 and S31 illustrate how electronic perturbations introduced by substituents *X* (*X* = –S$^-$, –SAuPPh$_3$, –SCH$_2$CH$_2$CO$_2$CH$_2$CH$_3$, –SH, –N≡CCr(CO)$_5$) at one terminus of the linear 6,6′-biazulenic framework modulate the electron density at its other end featuring the [(–NC)Cr(CO)$_5$] ^{13}C NMR reporter. The ^{13}C chemical shifts within the [(–NC)Cr(CO)$_5$] moiety reflect electron richness of the Cr centre, which is influenced by the nature of the remote substituent *X*. A raise in the net electron-donating strength of *X* (–S$^-$ > –SAuPPh$_3$ > –SCH$_2$CH$_2$CO$_2$CH$_2$CH$_3$ ≈ –SH > –N≡CCr(CO)$_5$) decreases $\delta(^{13}CN)$, with a concomitant increase in $\delta(^{13}CO)$ due to enhanced Cr(dπ) → CO(pπ*) back-bonding.[55] The $\delta(^{13}CO_{trans})$ or $\delta(^{13}CO_{cis})$ *versus* $\delta(^{13}CN)$ inverse-linear correlations (Fig. 8 and S31, respectively) exhibit excellent linearity. Thus, the ^{13}C NMR data quantitatively capture subtle, long-range substituent effects without relying on any vibrational metrics, establishing the [(–NC)Cr(CO)$_5$] fragment as a highly sensitive reporter of π-mediated electron delocalization across the 6,6′-biazulenic scaffold.

Self-assembly of mercaptobiazulene 15 on Au(111) surface

Immersion of four separate 1 × 1 cm^2 gold-coated silicon substrates with predominant Au(111) surface orientation into 2 mM $CHCl_3$ solutions of **15** for at least 24 hours produced self-assembled monolayers (SAMs) with ellipsometric thicknesses of 24.4 ± 2.1 Å, consistent with a terminal-upright molecular orientation and a "hollow-linear" Au–S binding mode[58] (Fig. S60a). The calculated thickness of 23.7 Å for an idealized linear Au–S–C geometry agrees closely with this value.

Formation of the Au–S interface is evidenced by the disappearance of the weak ν_{SH} band of **15**,[59] and by pronounced

changes in the ν_{CO} region. DFT calculations[48] and a large body of experimental evidence[48,52,55] suggests that for complexes [$(OC)_5Cr(CNR)$] in an isotropic environment (*i.e.*, solution phase), one of the two IR-active ν_{CO} bands of A_1 symmetry is typically obscured by a much more prominent ν_{CO} band of E symmetry. Upon approximately terminal-upright chemisorption, the $\nu_{CO}(E)$ band, which reflects vibration of the *cis*-CO ligands within the C_{4v}-symmetric [$Cr(CO)_5L$] unit, diminishes markedly to uncover the $\nu_{CO}(A_1^{(2)})$ feature (Fig. S60b and c). The $\nu_{CO}(A_1^{(2)})$ band arises chiefly from vibration of the *trans*-CO unit.[48,52] In addition, the relative intensity of the $\nu_{CO}(A_1^{(1)})$ band, which corresponds to the "breathing" mode of vibration of all five COs, decreases. These observations indicate preferential alignment of *cis*-CO oscillators parallel to the surface and suppression of the $\nu_{CO}(E)$ absorption under the surface IR selection rules.[60]

When SAMs of **15** are instead generated *via* displacement of the isocyanide-anchored biazulenic film shown in Fig. 9a,[35] the $\nu_{CO}(E)$ band nearly disappears, and the broad ν_{NC} band at 2175 cm^{-1} (gold-bound isocyanide) vanishes altogether, confirming replacement of the chemisorbed isocyanobiazulene by mercaptobiazulene (Fig. 9b and c). Thus, the monolayer displacement route produces a more vertically-packed film, likely reflecting steric confinement of the vacated surface sites[61,62] that are accessible only to vertically approaching molecules of **15**.

Both A_1-symmetric ν_{CO} bands of **15** undergo hypsochromic shifts upon SAM formation, with the $\nu_{CO}(A_1^{(2)})$ feature moving up by 23 cm^{-1} (Fig. S60b and c). This shift exceeds the experimental uncertainty in its ν_{max} value in the solution spectrum and suggests reduced Cr(dπ) → CO(pπ*) back-bonding in the SAM relative to free **15**. The diminished electron richness of the Cr(0) centre arises from S(3p) → Au π-bonding, which enhances the net acceptor character[52] of the isocyanobiazulene ligand. Thus, the thio-linked Au(111) surface acts as an electron-withdrawing moiety[35,48] transmitting its effect through the biazulenic π-linker to the distal Cr(0) site, approximately 2 nm away. In contrast, the –$SAuPPh_3$ fragment in the related heterobimetallic complex **16**, with the anticipated bent C–S–Au angle,[50] behaves as a net electron donor (Fig. 8). The above observations demonstrate that 6,6′-biazulene can serve as a molecular relay, communicating spectroscopically discernible electronic perturbations from a metallic surface to a remote metal centre.

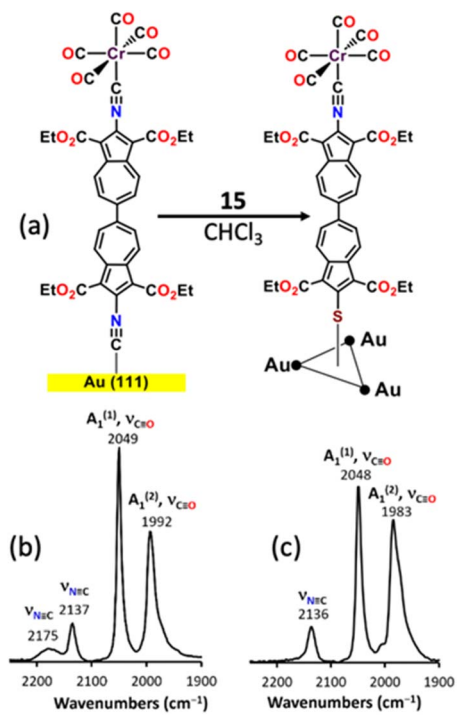

Fig. 9 (a) Formation of the SAM film of **15** on the Au(111) surface *via* SAM displacement protocol. (b) RAIR spectrum of the SAM of the preformed isocyanide-anchored 6,6′-biazulenic monolayer on Au(111). (c) RAIR spectrum of the resulting S-anchored SAM film of **15** upon displacement.

Conclusions

A family of previously inaccessible 6,6′-biazulenes, both symmetrically and asymmetrically functionalized along their molecular axis, was synthesized in this work. The 2,2′-dichloro-1,1′,3,3′-tetraethoxycarbonyl-6,6′-biazulene precursor proved to be a versatile synthon for accessing symmetrically functionalized derivatives through substitution at the 2,2′-positions. Of particular interest for the realm of π-conducting materials is the hitherto unknown 2,2′-dimercapto-1,1′,3,3′-tetraethoxycarbonyl-6,6′-biazulene **3**, which combines extended π-conjugation with surface anchoring capability. On the other hand, Suzuki–Miyaura cross-coupling provided a modular route to asymmetrically-functionalized 6,6′-biazulenes, permitting installation of electronically distinct substituents at the 2,2′-termini of the 6,6′-biazulenic framework. The calibration plot correlating the half-wave potential ($E_{1/2}$) for the one-step, 2-e^- reversible reduction of 2,2′-functionalized 6,6′-biazulenes with the sum of Hammett σ_p constants led to straightforward extraction of effective σ parameters for substituents lacking conventional σ_p descriptors. Using this calibration, a dual Hammett analysis was implemented: a reverse approach to derive effective σ constants electrochemically, followed by a direct correlation to predict reduction potentials of newly synthesized 6,6′-biazulenic derivatives. The excellent predictive accuracy of such bidirectional validation underscored the quantitative reliability of the linear free-energy relationships governing our 6,6′-biazulenic Hammett analyses. Our electrochemical analysis captured the effect of intramolecular C═O···H–S hydrogen bonding, which rendered the effective σ parameter for the mercapto group more negative than the commonly accepted σ_p value, reflecting its increased electron-donating capacity imparted through such non-Pauling H-bonding interaction.[63] Furthermore, considering the –NMe_2 substituent as a case study afforded direct access to its effective Hammett constant. A mild steric repulsion with the ethoxycarbonyl groups in **6** diminishes π-conjugative donation of –NMe_2, surprisingly leading to $\sigma_{eff}(NMe_2) > \sigma_{eff}(NH_2)$. Finally, we demonstrated how the [–$NCCr(CO)_5$] fragment serves as a highly responsive ^{13}C NMR and RAIR reporter, providing complementary insight into electron delocalization across the 6,6′-biazulenic π-linker.

Taken together, the synthetic, electrochemical, and spectroscopic findings reported herein offer an experimentally robust platform for systematically quantifying substituent effects. This platform transcends the classical benzenoid σ_p paradigm while remaining numerically anchored to it by design. By further enabling predictive mapping of electronic influence, our approach expands the palette for tailored design of redox-active molecules, π-linked materials, and electronically coupled interfaces. In a broader context, the 1,1′,3,3′-tetra-ethoxy-carbonyl-6,6′-biazulenic platform is most valuable for interrogating any substituents whose electronic influence is dominated by inductive effects rather than mesomeric π-conjugation, as well as for π-conjugating substituents that experience minimal steric interference. Our current efforts are directed toward the development of a second-generation 6,6′-biazulenic framework designed to avoid intramolecular hydrogen bonding and steric contributions, thereby further refining the extraction of effective Hammett σ values.

Author contributions

Conceptualization: M. V. B.; synthesis, characterization, and data analysis: J. A. M., S. R. K, J. C. A., R. C. S., and C. R. W.; surface studies: M. K. D. and C. L. B.; crystal structure solution and refinement: D. E. J.; computational work: R. F. and W. H. T.; supervision: M. V. B., C. L. B., and W. H. T.; original draft preparation: M. V. B., J. A. M., and S. R. K. All authors were involved in reviewing and editing the manuscript and have agreed to its published version.

Conflicts of interest

There are no conflicts to declare.

Data availability

CCDC 2482367 (**4**) contains the supplementary crystallographic data for this paper.[64]

Full experimental details, characterization and computational data are provided in the supplementary information (SI). Supplementary information is available. See DOI: https://doi.org/10.1039/d6ra00120c.

Acknowledgements

The authors thank Dr William W. Brennessel (University of Rochester) for valuable discussions and expert guidance on modelling crystallographic disorder in the X-ray structure of compound **4**. This research was funded by the US National Science Foundation grant CHE-1808120 to M. V. B. J. A. M. is thankful for the support provided by the J. K. Lee Summer Scholarship. S. R. K. acknowledges the support by the NSF Graduate Research Fellowship under grant DGE-1940699 and the Madison and Lila Self Graduate Fellowship. R. C. S. and C. R. W. were supported by the NSF REU Grants CHE-2349329 and CHE-1950293, respectively. R. F. is grateful for the Jack and Carolyn Landgrebe Summer Undergraduate Research Scholarship. Support for the NMR instrumentation was provided by NIH Shared Instrumentation Grants (S10OD016360 and S10RR024664) and an NIH Center Grant (P20 GM103418). The calculations were performed at the University of Kansas Center for Research Computing (CRC), including the BigJay cluster resource funded through NSF Grant No. MRI-2117449.

Notes and references

1 V. K. Yadav, *Steric and Stereoelectronic Effects in Organic Chemistry*, Springer, Singapore, 2021, pp. 179–189.
2 E. V. Anslyn and D. A. Dougherty, *Modern Physical Organic Chemistry*, University Science Books, Melville, 2005, pp. 445–471.
3 R. J. Mayer and D. Leboeuf, *Angew Chem. Int. Ed. Engl.*, 2025, e202516932, DOI: 10.1002/anie.202516932.
4 G. Kumar, L. Tibbitts, J. Newell, B. Panthi, A. Mukhopadhyay, R. M. Rioux, C. J. Pursell, M. Janik and B. D. Chandler, *Nat. Chem.*, 2018, **10**, 268–274.
5 A. J. Neel, M. J. Hilton, M. S. Sigman and F. D. Toste, *Nature*, 2017, **543**, 637–646.
6 M. T. Huynh, C. W. Anson, A. C. Cavell, S. S. Stahl and S. Hammes-Schiffer, *J. Am. Chem. Soc.*, 2016, **138**, 15903–15910.
7 L. T. Kanerva and A. M. Klibanov, *J. Am. Chem. Soc.*, 1989, **111**, 6864–6865.
8 S. Itoh and S. Fukuzumi, *Accounts Chem. Res.*, 2007, **40**, 592–600.
9 J. Serrano-Plana, I. Garcia-Bosch, A. Company and M. Costas, *Accounts Chem. Res.*, 2015, **48**, 2397–2406.
10 A. H. Brozena, M. Kim, L. R. Powell and Y. Wang, *Nat. Rev. Chem.*, 2019, **3**, 375–392.
11 M. N. Ates, C. J. Allen, S. Mukerjee and K. M. Abraham, *J. Electrochem. Soc.*, 2012, **159**, A1057–A1064.
12 E. W. Driscoll, J. R. Hunt and J. M. Dawlaty, *J. Phys. Chem. Lett.*, 2016, **7**, 2093–2099.
13 D. Chiodi and Y. Ishihara, *J. Med. Chem.*, 2023, **66**, 5305–5331.
14 N. H. Nguyen, J. W. Apriletti, J. D. Baxter and T. S. Scanlan, *J. Am. Chem. Soc.*, 2005, **127**, 4599–4608.
15 E. Y. Xu, A. Castanedo, N. Y. Shin, L. K. Valloli, D. C. Grills, M. J. Bird and R. R. Knowles, *J. Am. Chem. Soc.*, 2025, **147**, 21735–21742.
16 A. A. Adeniyi, T. L. Ngake and J. Conradie, *Electroanalysis*, 2020, **32**, 2659–2668.
17 N. G. S. Mateyise, M. M. Conradie and J. Conradie, *J. Electroanal. Chem.*, 2023, **947**, 117807.
18 M. Bragato, G. F. von Rudorff and O. A. von Lilienfeld, *Chem. Sci.*, 2020, **11**, 11859–11868.
19 G. Monteiro-de-Castro, J. C. Duarte and I. J. r. Borges, *J. Org. Chem.*, 2023, **88**, 9791–9802.
20 A. Yett and P. R. Rablen, *J. Phys. Org. Chem.*, 2023, **36**, e4436.
21 V. Saini and R. Kumar, *Artif. Intell. Chem.*, 2024, **2**, 100079.
22 V. Saini and R. Kumar, *Phys. Chem. Chem. Phys.*, 2025, **27**, 12951–12962.
23 I. Nikovskiy, D. Aleshin, A. Anisimov, V. Novikov and Y. Nelyubina, *Inorg. Chem. Front.*, 2025, **12**, 7795–7801.

24 G. Comas-Vilà and P. Salvador, *Phys. Chem. Chem. Phys.*, 2025, **27**, 10482–10491.
25 M. Shahamirian, P. A. Wieczorkiewicz, T. M. Krygowski and H. Szatylowicz, *J. Org. Chem.*, 2023, **88**, 7940–7952.
26 C. Hansch, A. Leo and R. W. Taft, *Chem. Rev.*, 1991, **91**, 165–195.
27 H. H. Jaffe, *Chem. Rev.*, 1953, **53**, 191–261.
28 D. H. Mcdaniel and H. C. Brown, *J. Org. Chem.*, 1958, **23**, 420–427.
29 J. Johnston, *Proc. Roy. Soc.*, 1906, **78**, 82–102.
30 S. Hunig and B. Ort, *Liebigs Ann. Chem.*, 1984, 1905–1935.
31 S. Hunig and B. Ort, *Liebigs Ann. Chem.*, 1984, 1936–1951.
32 S. Hunig, B. Ort, M. Hanke, C. Jutz, T. Morita, K. Takase, Y. Fukazawa, M. Aoyagi and S. Ito, *Liebigs Ann. Chem.*, 1984, 1952–1958.
33 S. Hunig and B. Ort, *Liebigs Ann. Chem.*, 1984, 1959–1971.
34 T. R. Maher, A. D. Spaeth, B. M. Neal, C. L. Berrie, W. H. Thompson, V. W. Day and M. V. Barybin, *J. Am. Chem. Soc.*, 2010, **132**, 15924–15926.
35 P. T. Connelly, J. C. Applegate, D. A. Maldonado, M. K. Okeowo, W. C. Henke, A. G. Oliver, C. L. Berrie and M. V. Barybin, *Dalton Trans.*, 2023, **52**, 11419–11426.
36 D. H. Evans, *Chem. Rev.*, 2008, **108**, 2113–2144.
37 M. J. Bird, T. Iyoda, N. Bonura, J. Bakalis, A. J. Ledbetter and J. R. Miller, *J. Electroanal. Chem.*, 2017, **804**, 107–115.
38 A. J. Fry, *Electroanalysis*, 2006, **18**, 391–398.
39 A. P. Gee, T. M. Gianga, G. Kociok-Köhn, G. Dan Pantos and S. E. Lewis, *RSC Adv.*, 2025, **15**, 14881–14892.
40 S. R. Kelsey, G. Griaznov, A. D. Spaeth, D. E. Janzen, J. T. Douglas, W. H. Thompson and M. V. Barybin, *Chem. Commun.*, 2024, **60**, 5213–5216.
41 N. G. Connelly and W. E. Geiger, *Chem. Rev.*, 1996, **96**, 877–910.
42 N. Elgrishi, K. J. Rountree, B. D. McCarthy, E. S. Rountree, T. T. Eisenhart and J. L. Dempsey, *J. Chem. Educ.*, 2018, **95**, 197–206.
43 B. M. Neal, A. S. Vorushilov, A. M. DeLaRosa, R. E. Robinson, C. L. Berrie and M. V. Barybin, *Chem. Commun.*, 2011, **47**, 10803–10805.
44 C. Y. Zhang, J. Cheng, Q. Q. Wu, S. J. Hou, S. Feng, B. Jiang, C. J. Lambert, X. K. Gao, Y. Q. Li and J. H. Li, *J. Am. Chem. Soc.*, 2023, **145**, 1617–1630.
45 T. Nozoe, S. Seto and S. Matsumura, *Bull. Chem. Soc. Jpn.*, 1962, **35**, 1990–1998.
46 N. Miyaura, K. Yamada and A. Suzuki, *Tetrahedron Lett.*, 1979, **20**, 3437–3440.
47 H. S. Xin, C. W. Ge, X. D. Yang, H. L. Gao, X. C. Yang and X. K. Gao, *Chem. Sci.*, 2016, **7**, 6701–6705.
48 J. C. Applegate, M. K. Okeowo, N. R. Erickson, B. M. Neal, C. L. Berrie, N. N. Gerasimchuk and M. V. Barybin, *Chem. Sci.*, 2016, **7**, 1422–1429.
49 H. Häkkinen, *Nat. Chem.*, 2012, **4**, 443–455.
50 K. J. Scheetz, A. D. Spaeth, A. S. Vorushilov, D. R. Powell, V. W. Day and M. V. Barybin, *Chem. Sci.*, 2013, **4**, 4267–4272.
51 T. C. Holovics, R. E. Robinson, E. C. Weintrob, M. Toriyama, G. H. Lushington and M. V. Barybin, *J. Am. Chem. Soc.*, 2006, **128**, 2300–2309.
52 M. D. Hart, J. Meyers, Z. A. Wood, T. Nakakita, J. C. Applegate, N. R. Erickson, N. N. Gerasimchuk and M. V. Barybin, *Molecules*, 2021, **26**, 981.
53 D. L. DuBose, R. E. Robinson, T. C. Holovics, D. R. Moody, E. C. Weintrob, C. L. Berrie and M. V. Barybin, *Langmuir*, 2006, **22**, 4599–4606.
54 H. Gilman and G. E. Dunn, *J. Am. Chem. Soc.*, 1951, **73**, 3404–3407.
55 A. E. Carpenter, C. C. Mokhtarzadeh, D. S. Ripatti, I. Havrylyuk, R. Kamezawa, C. E. Moore, A. L. Rheingold and J. S. Figueroa, *Inorg. Chem.*, 2015, **54**, 2936–2944.
56 D. Karakas and C. Kaya, *J. Organomet. Chem.*, 2001, **640**, 37–40.
57 A. Hinchliffe and H. J. Soscún, *Chem. Phys. Lett.*, 2005, **412**, 365–368.
58 M. Tachibana, K. Yoshizawa, A. Ogawa, H. Fujimoto and R. Hoffmann, *J. Phys. Chem. B*, 2002, **106**, 12727–12736.
59 S. H. Choi, B. Kim and C. D. Frisbie, *Science*, 2008, **320**, 1482–1486.
60 H. A. Pearce and N. Sheppard, *Surf. Sci.*, 1976, **59**, 205–217.
61 J. J. Yu, Y. H. Tan, X. Li, P. K. Kuo and G. Y. Liu, *J. Am. Chem. Soc.*, 2006, **128**, 11574–11581.
62 S. Xu, P. E. Laibinis and G. Y. Liu, *J. Am. Chem. Soc.*, 1998, **120**, 9356–9361.
63 J. K. Wang, C. H. Wang, C. C. Wu, K. H. Chang, C. H. Wang, Y. H. Liu, C. T. Chen and P. T. Chou, *J. Am. Chem. Soc.*, 2024, **146**, 3125–3135.
64 CCDC 2482367 (**4**): Experimental Crystal Structure Determination, 2026, DOI: 10.5517/ccdc.csd.cc2pb3cj.